Computational Local Helioseismology in the Frequency Domain

Chris S. Hanson[1], Michael Leguèbe[1], Damien Fournier[2], Aaron C. Birch[1] & Laurent Gizon[1,3]

[1]Max-Planck-Institut für Sonnensystemforschung, Göttingen, Germany
[2]Institut für Numerische und Angewandte Mathematik, Göttingen, Germany
[3]Institut für Astrophysik, Georg-August-Universität Göttingen, Germany

in collaboration with **Inria team Magique3D**,
Inria Bordeaux Sud-Ouest, France

Forward problems in local helioseismology have thus far been addressed in a semi-analytical fashion using the Born approximation and normal-mode expansions or direct simulations. However, it has proven difficult to take into account geometrical and instrumental effects. To avoid these difficulties we employ a numerical method to determine the impulse response of a solar model in a 2.5D geometry. Solving the wave equation in the frequency domain avoids the difficulties (instabilities) faced in the time domain. This framework is flexible, computationally efficient, and produces solar-like power spectrum and cross-covariance that agree reasonably with observations, including the high-frequency continuous spectrum. Additionally, we present accurate travel-time sensitivity kernels for perturbations to the solar medium which hint at the promising potential of this framework in future forward and inversion problems.

Wave Propagation in Axially Symmetric Solar Models

In order to describe wave propagation in the sun, we compute the Green's function G which is the response to a point source at any arbitrary location. It is defined as the solution to

$$\mathscr{L}G(t,\boldsymbol{r},\boldsymbol{r_s}) = \delta(t-t_0)\delta(\boldsymbol{r}-\boldsymbol{r}_s),$$

where $\mathscr{L}$ is a linear operator modelling solar wave propagation. The point source of the oscillations is located at $\boldsymbol{r}_s$ and at time t_0.

In frequency space, we consider a simple scalar wave operator that allows fast computation while capturing the essential physics of acoustic waves in the sun:

$$\mathscr{L}G_\omega = \left(\omega^2 + 2i\omega\gamma\right)G_\omega + 2i\omega\boldsymbol{u}\cdot\nabla G_\omega + c\nabla\cdot\left(\frac{1}{\rho}\nabla(\rho c G_\omega)\right) = -\delta(\boldsymbol{r}-\boldsymbol{r}_s), \tag{1}$$

where $G_\omega = c\nabla\cdot\boldsymbol{\xi}_\omega$ is linked to the divergence of the fluid displacement, within an atmosphere of density ρ and sound speed c. Additionally, the waves are attenuated at a rate of γ. For simplicity, we have neglected gravity terms and consider a first-order advection term where the flow $\boldsymbol{u}$ is mass conservative (i.e. $\nabla\cdot\rho\boldsymbol{u}=0$).

The fundamental quantity for local helioseismology is the cross-covariance of the seismic wavefield. In particular the cross-covariance of the oscillations between two observation points $(\boldsymbol{r}_1,\boldsymbol{r}_2)$ can be written, under the assumption that sources are spatially uncorrelated, as

$$\overline{C}(\boldsymbol{r}_1,\boldsymbol{r}_2,\omega) = \int_V\int_{V'} G^*(\boldsymbol{r}_1,\boldsymbol{r})G(\boldsymbol{r}_2,\boldsymbol{r}')M(\boldsymbol{r},\boldsymbol{r}')\rho\mathrm{d}\boldsymbol{r}\rho'\mathrm{d}\boldsymbol{r}' \tag{2}$$

where the source of excitation is specified through,

$$M(\boldsymbol{r},\boldsymbol{r}',\omega) = \epsilon(\boldsymbol{r})P_s(\omega)\delta(\boldsymbol{r}-\boldsymbol{r}'). \tag{3}$$

where $\epsilon(\boldsymbol{r})$ and $P_s(\omega)$ control the spatial and frequency dependencies of the source covariance, respectively. Equation 2 is an essential quantity, but is far from trivial to compute. Here we adopt a different strategy to compute $\overline{C}$. Specifically, does there exist a source covariance such that $\overline{C}$ can be described in terms of the Green's function, as is done in geophysics [1]?

We first define a generalized seismic reciprocity, whereby the same signal is observed whether $\boldsymbol{r}_1$ and $\boldsymbol{r}_2$ are interchanged or not. Specifically,

$$G(\boldsymbol{r}_2,\boldsymbol{r}_1;\boldsymbol{u}) = G(\boldsymbol{r}_1,\boldsymbol{r}_2;-\boldsymbol{u}), \tag{4}$$

where the sign of $\boldsymbol{u}$ indicates the direction of flow. With this generalization in hand, the expectation value of the cross covariance is then related to the Green's function through

$$\overline{C}_\omega(\boldsymbol{r}_1,\boldsymbol{r}_2,\boldsymbol{u}) = \frac{P_s(\omega)}{4i\omega}\left[G_\omega(\boldsymbol{r}_2,\boldsymbol{r}_1;\boldsymbol{u}) - G^*_\omega(\boldsymbol{r}_2,\boldsymbol{r}_1;-\boldsymbol{u})\right], \tag{5}$$

under the assumption of that the source covariance amplitude takes the form of

$$\epsilon(\boldsymbol{r}) = \frac{\gamma(\boldsymbol{r},\omega)}{\rho(\boldsymbol{r})} + \frac{c}{2\rho}\delta(r-R(\theta)). \tag{6}$$

To simplify the forward problem in local helioseismology it would be nice if equation 5 holds. Does it give a reasonable power spectrum? To determine this we first need to solve equation 1 in a reasonably efficient manner.

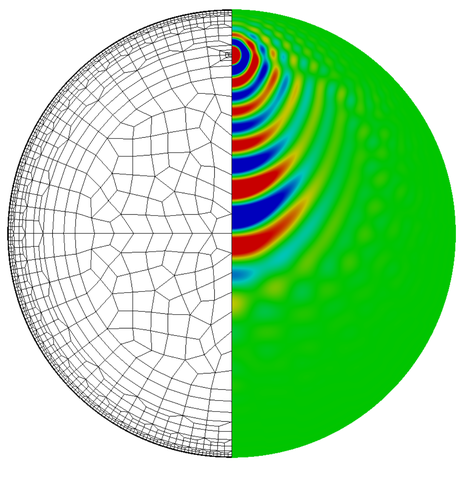

Figure 1: Illustrations of (left) the computational mesh used by the finite element regime and (right) the imaginary part of the Green's function with the Dirac source located at a distance of $0.8R_\odot$ along the z-axis

Axially Symmetric Problem: We consider an axially-symmetric background model and flow and thus can decompose our problem into individual 2D problems for each Fourier mode m,

$$G_\omega(r,\theta,\phi,\boldsymbol{r_s}) = \sum_m G^m_\omega(r,\theta,\boldsymbol{r_s})e^{im\phi}, \tag{7}$$

and reconstruct the solution into 3D in post-treatment. This problem is 'embarrassingly parallel' in both frequency and azimuthal mode, allowing for very efficient computation.

In our case we perform the computations using the *Montjoie* solver, which is based on the finite elements method. The solution is obtained on a computational mesh consisting of small cells in which the solution is projected onto high-degree polynomials (see figure 1). Due to the rapid changes in the sound speed and density near the surface we refine the mesh accordingly. A Neumann boundary condition $(\partial_n G_\omega = 0)$ is imposed upon the polar axis and a Sommerfeld boundary condition $(\partial_n G_\omega = ikG_\omega)$ on the outer radial edge (c.f. Leguèbe et al. Poster).

Power Spectra

In order to assess the validity of our convenient source covariance (Eq. 5), we compare the power spectra and cross-covariance obtained from *Montjoie* with that which is observed on the solar surface. We compute the power spectrum $\mathscr{P}_{lm}$ for each azimuthal mode m and degree l through a spherical harmonic transform of the cross-covariance function,

$$\begin{aligned}\mathscr{P}_{lm}(\omega) &= \int_0^{2\pi}\int_0^{\pi}\overline{C}_\omega(\theta)Y^m_l(\theta,\phi)\sin\theta\ \mathrm{d}\theta\mathrm{d}\phi,\\ &= \frac{P_s(\omega)}{2\omega}\int_0^{2\pi}\int_0^{\pi}\mathrm{Im}G_\omega(\theta)Y^m_l(\theta,\phi)\sin\theta\ \mathrm{d}\theta\mathrm{d}\phi.\end{aligned} \tag{8}$$

where the last equality is derived from a background without flow $(\boldsymbol{u}=0)$. Figures 2 and 3 show the power spectra with no background flow and a differential rotation profile, respectively. The comparisons show good agreement between the simulated power spectra ridge positions with those reported by [2] and [3]. While there is general agreement we note that due to the chosen background parameters (model S) the mode frequencies overestimate those in the observations [5]. Comparisons of a simulated temporal cross-covariance (time-distance diagram) and that which was reported by [4] agree well with the low number skip branches, but there is still some improvement needed in fine tuning the source covariance amplitude to improve agreement for higher skip branches.

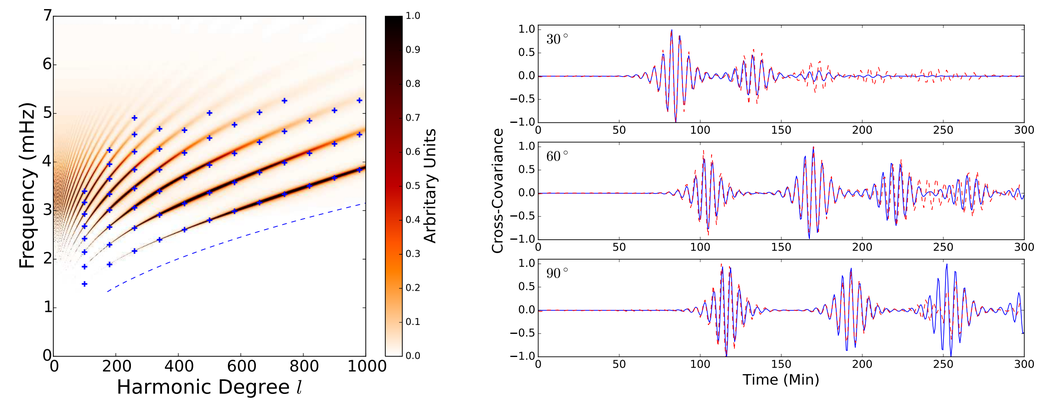

Figure 2: Top: l-ν power spectrum of the waves computed at the solar surface with no background flow. The blue crosses indicate the position of the $p_1 - p_8$ modes reported by [2], while the blue dashed line shows the observed f-mode ridge which is missing in this simulation due to the lack of a gravitational term. Right: Temporal cross-covariance function for three angular distances $30°$, $60°$, and $90°$ for the simulations (blue) and the MDI/SOHO/Doppler observations [red dashes, 4].

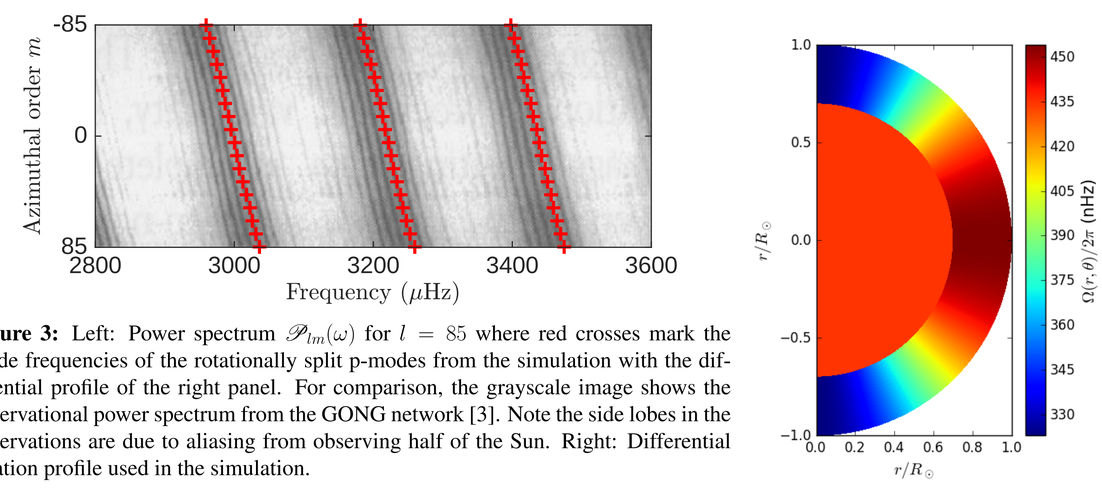

Figure 3: Left: Power spectrum $\mathscr{P}_{lm}(\omega)$ for $l = 85$ where red crosses mark the mode frequencies of the rotationally split p-modes from the simulation with the differential profile of the right panel. For comparison, the grayscale image shows the observational power spectrum from the GONG network [3]. Note the side lobes in the observations are due to aliasing from observing half of the Sun. Right: Differential rotation profile used in the simulation.

Travel-Time Sensitivity Kernels

In the presence of perturbations to the background model, a perturbation in $\mathscr{L}$ occurs which enables the computation of the change in $\overline{C}$. We compute this change $\overline{\delta C}$ and determine the corresponding travel-time difference $\delta\tau$ through,

$$\delta\tau(\boldsymbol{r}_1,\boldsymbol{r}_2) = \int_{-\infty}^{\infty} W^*(\omega)\overline{\delta C}(\boldsymbol{r}_1,\boldsymbol{r}_2)\ \mathrm{d}\omega \tag{9}$$

where W is a weighting function of the unperturbed cross-covariance function. Forward modelling of perturbations to the background can produce travel times that are directly comparable to those obtained from observations and thus enable the testing of models.

However, as is more often the case in reality, the subsurface structures within the sun that cause observed travel time differences are unknown or disagree with current models. In order to understand the spatial sensitivity of travel times to these structures, the development of travel time sensitivity kernels K for each background parameter α is required. This is achieved though the expansion of the perturbed wave operator to first order (first Born approximation) and the use of $\overline{C}$ and G,

$$\begin{aligned}K_\alpha(\boldsymbol{r}_1,\boldsymbol{r}_2,\boldsymbol{r}) = &-\int_{-\infty}^{\infty} W^*\mathcal{L}_\alpha[G(\boldsymbol{r},\boldsymbol{r}_2),\overline{C}(\boldsymbol{r},\boldsymbol{r}_1)]\mathrm{d}\omega\\ &-\int_{-\infty}^{\infty} W^*\mathcal{L}^*_\alpha[G^*(\boldsymbol{r},\boldsymbol{r}_1),\overline{C}^*(\boldsymbol{r},\boldsymbol{r}_2)]\mathrm{d}\omega\end{aligned} \tag{10}$$

where $\mathcal{L}_\alpha$ is a bilinear operator dependant upon the model parameters. For each background parameter the bilinear operator $\mathcal{L}_\alpha$ is simple and can be found in [6]. The advantage of the convenient source covariance is that Eq. 10 combined with Eq 5 makes the computation of the kernels straightforward and efficient, unlike previous works (eg. [7]).

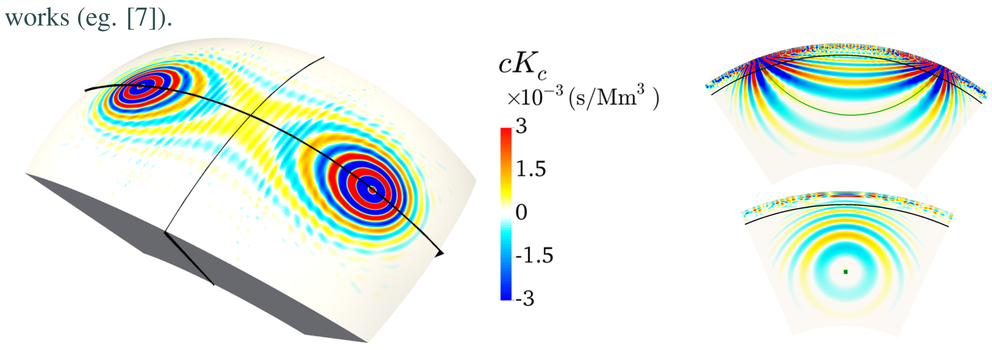

Figure 4: Mean travel-time sensitivity kernel for sound speed (multiplied by c) between point $\boldsymbol{r}_1$ located on the polar axis and point $\boldsymbol{r}_2$ at latitude of $45°$. Left: Cut through the sound-speed kernel cut at radius $r = 0.95R_\odot$. Top Right: Slice through a plane containing the two observation points and the centre of the Sun. The green line indicates the position of the ray path. Bottom Left: Slice in a plane perpendicular to the ray path connecting the two observation points (green square), at equal distance from the two observation points. In both right hand slices, the black arc of a circle locates radius $r = 0.95R_\odot$ which corresponds to the left panel.

So What Next?

Forward modelling – The present set-up can be very useful to test new methods, include various instrumental and projection effects, but also to interpret existing travel-time measurements for rotation, meridional circulation, and axisymmetric structures like the average supergranule.

Inversions – Find the parameters $\delta\alpha$ of the background model (sound speed, density, flows) such that the travel times from the model are consistent with the observed travel times through the use of non-linear inversions or the iterative application of the kernels.

References

[1] R. Snieder, M. Miyazawa, E. Slob, I. Vasconcelos, and Kees Wapenaar. A comparison of strategies for seismic interferometry. *Surv. Geophys.*, 30(4):503–523, 2009.

[2] S. G. Korzennik, M. C. Rabello-Soares, J. Schou, and T. P. Larson. Accurate characterization of high-degree modes using mdi observations. *Astrophys. J.*, 772:87, August 2013.

[3] F. Hill, P. B. Stark, R. T. Stebbins, et al. The Solar Acoustic Spectrum and Eigenmode Parameters. *Science*, 272:1292–1295, May 1996.

[4] A. G. Kosovichev, T. L. Duvall, Jr., and P. H. Scherrer. Time-Distance Inversion Methods and Results - (Invited Review). *Solar Phys.*, 192:159–176, March 2000.

[5] C. S. Rosenthal, J. Christensen-Dalsgaard, Å. Nordlund, R. F. Stein, and R. Trampedach. Convective contributions to the frequencies of solar oscillations. *Astron. Astrophys.*, 351:689–700, November 1999.

[6] L. Gizon, H. Barucq, M. Duruflé, C.S. Hanson, M. Leguèbe, A.C. Birch, J. Chadbassier, D. Fournier, and T. Hohage. Computational helioseismology in the frequency domain: Acoustic waves in axisymmetric solar model with flows. *Astron. Astrophys.*, In Preparation, 2016.

[7] A. C. Birch, A. G. Kosovichev, and T. L. Duvall, Jr. Sensitivity of Acoustic Wave Travel Times to Sound-Speed Perturbations in the Solar Interior. *Astrophys. J.*, 608:580–600, June 2004.